Hindawi
Advances in Civil Engineering
Volume 2020, Article ID 8856987, 17 pages
https://doi.org/10.1155/2020/8856987

Research Article

Influential Factors of the Static Shear Properties of Coral Mud in the South China Sea

Yang Shen[1,2], **Xiaoxi Rui**[1,2], **Long Yang**[1,2], **Shaoyu Li**[1,2] and **Xue Shen**[1,2]

[1]*Key Laboratory of Geomechanics and Embankment Engineering of Ministry of Education, Hohai University, Nanjing 210024, China*
[2]*Jiangsu Research Center for Geotechnical Engineering Technology, Hohai University, Nanjing 210024, China*

Correspondence should be addressed to Xiaoxi Rui; 18251877144@163.com

Received 10 May 2020; Revised 2 August 2020; Accepted 11 August 2020; Published 24 August 2020

Academic Editor: Castorina S. Vieira

Coral mud, a kind of special material used for constructing islets in reclamation projects, is widely spread in the South China Sea. Combined with microstructure research, a series of triaxial tests were performed in this paper to study the static shear strength characteristics and potential factors that can influence them. The effective stress path was similar to the total stress path because of the unique microstructure resulting in a high strength and a high dissipation rate of the pore pressure in the coral mud. The initial void ratio and the initial confining pressure affected the strength and deformation characteristics of the coral mud. When the soil came to failure, the pore pressure coefficient A_f varied linearly with the initial void ratio. The critical friction angle was greatly influenced by the confining pressure, and its magnitude first developed to a peak value and then decreased as the void ratio increased. This change showed that there was a linear relationship between the initial elastic modulus E_{0i} and $\lg p_0$ as well as between the secant modulus E_{50} and p_0. The estimation ability of Cam-Clay was verified in this research. The value of parameter λ was determined incrementally by a larger initial void ratio, while the value of parameter M decreased smoothly first and then rose slightly; the selection of parameter κ was approximately 0.0035. The results supported that the Cam-Clay model is able to simulate the stress-strain relationship of coral mud, and a referenced estimation can be reliably and efficiently obtained for the reclamation projects of constructing islets.

1. Introduction

The South China Sea covers a vast area and enjoys a superior geographical location and strategic position [1]. In recent years, China has accelerated the development and utilization of coral reefs in the South China Sea. During the filling process, calcareous soil with large particles is first deposited at the bottom under gravity, while small particles, referred to as coral mud, are suspended in the water to form silty sand after drifting [2]. According to the national panel survey, coral mud is one of the most important submarine sediments in the eastern part of the South China Sea, accounting for 6.12% of the total sediments [3]. In addition, because of the intermittent construction of the filling operation, the coral soil layer presents a discontinuous distribution in the foundation. As a weak interlayer whose settlement and bearing capacity will inevitably affect the whole foundation, it is necessary to conduct in-depth and systematic research on the shear characteristics of coral mud to provide scientific and reasonable design parameters for the engineering construction of coral reefs.

The mineral composition of coral mud is similar to that of calcareous sand, with up to 96% calcium carbonate. A large number of research studies have been devoted to investigating the factors influencing the shear properties of calcareous sand, including the confining pressure, density, particle breakage [4], and shear rate [5]. Studies have found that the shear characteristics of calcareous sand are greatly dependent on the confining pressure [6]. If the confining pressure increases, then the strain under peak stress increases [7], and the initial response under a low confining pressure is rigid, with an obvious yield point and strain

hardening stage [8]. The impact of dilatancy on shear strength is far greater than that caused by particle breakage [9, 10].

According to particle size classification, coral mud is silty or silty clay. Geotechnical tests have shown that the water content is an important factor influencing the shear properties of clay and silt. Zhang et al. [11, 12] proposed the influence of the water content on red clay; specifically, with an increase in the water content, the peak cohesion and residual cohesion decrease, and the strain changes from softening to hardening. Xu et al. [13, 14] found that the pore pressure and cohesion increase when Shanghai soft soil is damaged. Feng et al. conducted a series of tests on silty clay and found that the failure shear strain value of silty soil decreases with increasing water content [15], and strain softening shows a weakening trend [16]. Wang et al. [17] found that the relationship between the cohesion and water content of calcareous silt can be represented by an M-shaped curve. The water contents corresponding to the two peaks of the M-type curve increase with increasing dry density.

At present, research on coral mud is scarce and has mostly been focused on the permeability sedimentary aspects. Shen et al. [18] considered the initial concentration to have a significant impact on the isovelocity deposition time of the coral mud. Wang [2] found that the coefficient of permeability of coral mud decreases with increasing density when the initial moisture content remains the same and reaches a maximum at saturation. Based on the existing research of calcareous sand and silty clay, the effects of the confining pressure and water content on coral mud were studied. Considering that, in the saturated triaxial test, the water content can be controlled by the initial void ratio [19] and the initial void ratio is a parameter of the Cam-Clay model, in this paper, the initial confining pressure and the initial void ratio were taken as variables. Taizhou soil was used as the control group. The applicability of the Cam-Clay model was discussed by comparing the simulation results with the experimental results.

2. Materials and Methods

Based on laboratory experiments, the static shear characteristics of coral mud samples were measured and compared with those of Taizhou soil in Zhejiang Province. The testing results are presented and discussed with respect to the following: (1) stress-strain relationship, (2) pore pressure development, (3) stress path, (4) friction angle (e.g., mobilized friction angle, critical state friction angle, and peak state friction angle), (5) modulus (e.g., initial elastic modulus and secant modulus), and (6) estimation ability of the Cam-Clay model.

2.1. Physical Characteristics of Materials. The coral mud for testing was obtained from the seabed of a reef in the South China Sea. Coral mud is a loose, unconsolidated, powdery deposit, light yellow to white in colour. To highlight the unique physical and mechanical characteristics of coral mud, Taizhou soil with similar liquid limits, plastic limits, and particle gradations was selected for comparison in consolidated undrained triaxial tests. The images of coral mud and Taizhou soil are provided in Figure 1.

An X-ray diffractometer was used to analyse the mineral composition and tabulate the results in Table 1. Figure 2 presents the distributions of each soil particle size. According to the standard [20], coral mud is silty clay, with a uniformity coefficient of $Cu = 37.5$ and coefficient of curvature $Cc = 0.4$; it is classified as poorly graded soil. Table 2 provides the basic characteristics.

2.2. Microstructure of the Materials. The microstructures of coral mud and Taizhou soil were magnified by 50 k with scanning electron microscopy (SEM). As shown in Figure 3(a), the granule morphology consisted of mainly strips and needles, with a small amount of irregular particles and obvious pore development. Figure 3(b) shows that most particles of Taizhou soil were clustered together in the form of aggregates, where small particles were attached on the surface of the large particles, mainly in face-to-face contact.

Forty representative particles were randomly selected to obtain the shape parameter circular degree R and ring diameter ratio T [21–23]. R measures the edges and corners. When $R = 1$, the particle is round. T represents the ratio of the longest axis to the shortest axis of the particle. The larger the value is, the closer the particle is to the dendritic shape [24]. As shown in Figure 4, $R_{(\text{coral mud})}$ is mainly distributed between 0.58 and 0.74, while T is between 3.12 and 4.87, consistent with the statistical average values of R and T (0.687 and 4.178). Compared with the mean values of R (0.915) and T (1.512) in Taizhou soil, the particle morphology of coral mud is extremely irregular due to its special sedimentary environment and chemical composition.

2.3. Testing Program. In this study, we first used X-ray diffraction and SEM to understand the chemical composition and microscopic fabric of the testing materials. After that, the effects of the initial confining pressure and initial void ratio on the shear properties were investigated by CU shear tests.

The apparatus used in the triaxial tests was an LSY30-1 stress-strain controlled triaxial instrument. The samples were evenly mixed and stored in a humidor for 24 h before being divided into five layers with the same mass and height. After 24 h of vacuum saturation, the samples were loaded into a pressure chamber, and then the reverse pressure saturation method was adopted until $\Delta u/\Delta\sigma_3 > 0.98$. The specimen has a diameter of 39.1 mm, a height of 80 mm, and an axial shear rate of 0.04 mm/min. The testing program is provided in Table 3.

3. Results and Discussion

3.1. Stress-Strain Relationship

3.1.1. Effects of the Initial Confining Pressure. The initial void ratio was 0.83, and CU shear tests were performed on the coral mud and Taizhou soil under four confining pressures

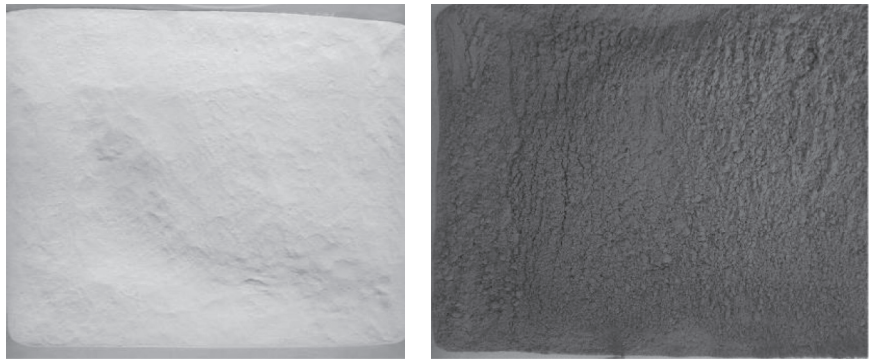

(a) (b)

Figure 1: Images of (a) coral mud and (b) Taizhou soil.

Table 1: Mineral composition of coral mud and Taizhou soil.

Type	Mineral composition		Chemical component			
	Percentage mass of various minerals (Wt, %)		Percentage of mass of each element (Wt, %)			
Coral mud	Biogenic calcium carbonate	$(Mg._{129}Ca._{871})\ CO_3$	Ca	Mg	O	C
	60.6	39.4	38.7	1	48.3	12.1
Taizhou soil	SiO_2	$(Mg_{0.03}Ca_{0.97})\ CO_3$	Ca	Si	O	C
	92.7	7.3	2.9	43.3	52.9	0.9

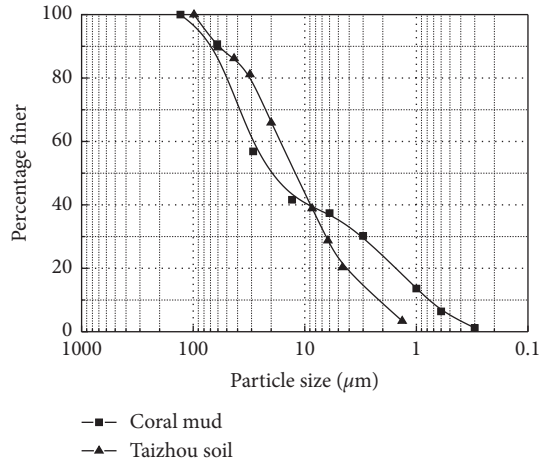

Figure 2: Particle size distribution.

Table 2: Basic characteristics of coral mud and Taizhou soil.

Type	Specific gravity Gs	Liquid limit w_L/%	Plastic limit w_p/%	Plastic index I_p/%
Coral mud	2.77	33.8	23	10.8
Taizhou soil	2.71	33.4	22.4	11.0

of 100 kPa, 200 kPa, 300 kPa, and 400 kPa (backpressure 50 kPa). The stress-strain behaviours are given in Figure 5. The strengths of the two soil samples both significantly increase with increasing confining pressure, especially the strength of the coral mud of adjacent confining pressure, which increases by nearly 500 kPa. The strength of coral mud was much higher than that of Taizhou soil under the same confining pressure. For a quantitative comparison, we calculated the c and φ of the two soil samples and calculated the mean values (Table 4). The mean internal friction angle of Taizhou soil is 15°, in line with the values of engineering experience, which is generally 15° to 25° but far smaller than those of coral mud. This result could be attributed to the slip-like structure and unique physicochemical properties of

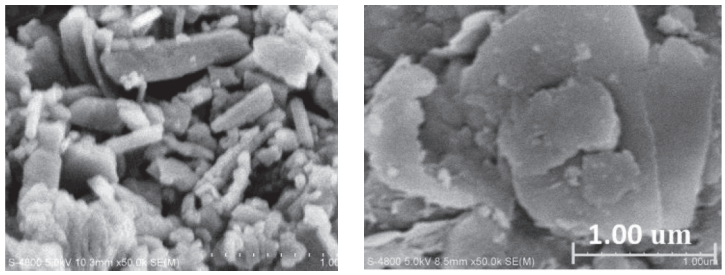

(a) (b)

Figure 3: SEM image of the testing materials: (a) coral mud and (b) Taizhou soil.

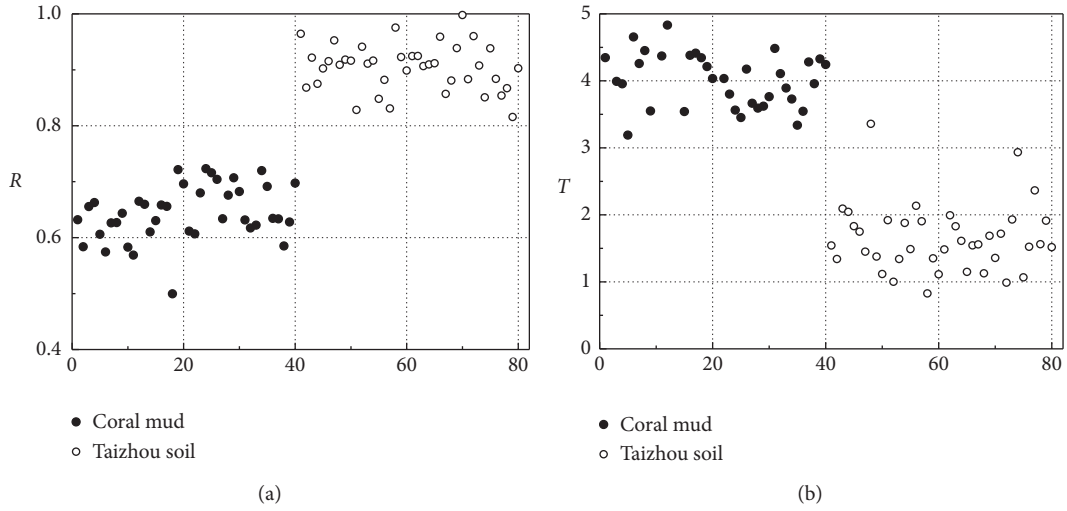

(a) (b)

Figure 4: Shape parameters of the testing materials: (a) circular degree and (b) ring diameter ratio.

coral mud, making the bite force generated by interparticle embedding large and strong.

In addition, the stress-strain growth trends of the two are also significantly different. The stress of coral mud increases rapidly at the initial stage of shear; when ε is 1%, the stress reaches approximately 2/3 of the shear strength, and the elastic modulus in the early stage is positively correlated with the confining pressure. In contrast, only when the confining pressure is 100 kPa does the Taizhou soil curve show a platform. The stress under other confining pressures stabilizes or even slightly decreases at approximately 50 kPa before $\varepsilon = 2\%$ and increases sharply between 2% and 3%. After $\varepsilon = 3\%$, the stress shows an increase with a steady rate whose amplitude accounts for 1/4 to 1/2 of the total stress.

From a microperspective, this increase could be a result of various particle contact responses. Previous studies [25, 26] have shown that the contact between particles includes frictional contact and cemented contact. The contact of Taizhou soil is cemented contact, and its stress-strain behaviour can be divided into the following three stages: (1) the OA stage where the stress increases linearly, (2) the AB stage where cement begins to break or extrude in which the stress develops smoothly or even declines at this stage, and (3) the BC stage where particles come into direct contact. The stress increases rapidly at this stage, and its growth rate is greater than that at the OA stage. Due to the lack of cementing materials, coral mud skips the OA and AB stages. Its irregular particles come into direct contact from the beginning, and the stress levels off after a rapid increase.

3.1.2. Effects of the Initial Void Ratio. Figure 6 shows the stress-strain relationship with different initial void ratios of coral mud and Taizhou soil. For Taizhou soil, the stress-strain behaviours of different e_0 values are roughly the same as the deviatoric stress rising by a small margin with a decrease in e_0. In addition, the strain when the stress surges declines with decreasing e_0, which means that the cement is more likely to be extruded and the particles are more likely to come into direct contact with each other under high dry density conditions. In contrast, the coral mud is more significantly affected, manifested as the diverse variation trend as well as the D-value, which can reach 500 kPa. When $e_0 = 0.89$, the stress-strain plot is obviously different in that it is an enhanced curve whose peak stress is higher than $e_0 = 0.83$ under different confining pressures. From the perspective of elastoplasticity, when the pressure increases, the coral mud with a large porosity transits from the elastic stage to the ideal plastic stage where part of the structure is broken. Its particles are more prone to particle dislocation

Table 3: Program of CU shear tests.

Number	p_0 (kPa)	ρ_d (g/cm^3)	e_0	w_0 (%)
CMA01	100	1.47	0.89	32
CMA02	200	1.47	0.89	32
CMA03	300	1.47	0.89	32
CMA04	400	1.47	0.89	32
CMA05	600	1.47	0.89	32
CMB01	100	1.51	0.83	30
CMB02	200	1.51	0.83	30
CMB03	300	1.51	0.83	30
CMB04	400	1.51	0.83	30
CMC01	100	1.56	0.78	28
CMC02	200	1.56	0.78	28
CMC03	300	1.56	0.78	28
CMC04	400	1.56	0.78	28
CMD01	100	1.64	0.69	25
CMD02	200	1.64	0.69	25
CMD03	300	1.64	0.69	25
CMD04	400	1.64	0.69	25
TZA01	100	1.47	0.89	32
TZA02	200	1.47	0.89	32
TZA03	300	1.47	0.89	32
TZA04	400	1.47	0.89	32
TZB01	100	1.51	0.83	30
TZB02	200	1.51	0.83	30
TZB03	300	1.51	0.83	30
TZB04	400	1.51	0.83	30
TZC01	100	1.64	0.69	25
TZC02	200	1.64	0.69	25
TZC03	300	1.64	0.69	25
TZC04	400	1.64	0.69	25

p_0 means initial confining pressure, ρ_d means dry density, e_0 means initial void ratio, and w_0 means initial moisture content.

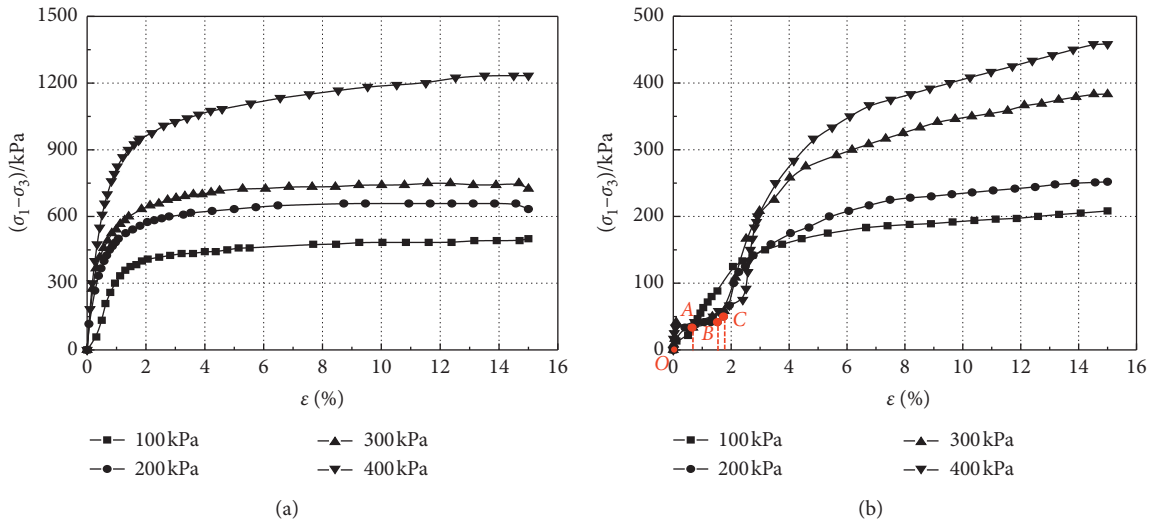

Figure 5: Stress-strain behaviour under four confining pressures: (a) coral mud and (b) Taizhou soil.

and rearrangement, which fills the pores and brings about a growth in the shear strength when $e_0 = 0.89$ [27]. Taizhou soil has no such feature owing to its shape and cementing substance, which do not facilitate maloperation and occlusion friction compared with needle-like particles [28].

3.2. Pore Pressure Development

3.2.1. Effects of the Initial Confining Pressure. In this part, we controlled $e_0 = 0.69$ to study the development law of the pore pressure under different confining pressures. As shown in

Table 4: Coulomb-molar parameters of coral mud and Taizhou soil.

Type	c_1 (kPa)	c_2 (kPa)	c_3 (kPa)	c_4 (kPa)	c_5 (kPa)	c_6 (kPa)	c (kPa)	φ_1	φ_2	φ_3	φ_4	φ_5	φ_6	φ
Coral mud	122.65	123.91	68.85	168.34	2.94	1.59	81.38	23°	21°	33°	18°	37°	46°	27.9°
Taizhou soil	67.62	46.16	54.79	2.01	36.3	15.03	53.65	11°	17°	15°	22°	16°	9°	15.0°

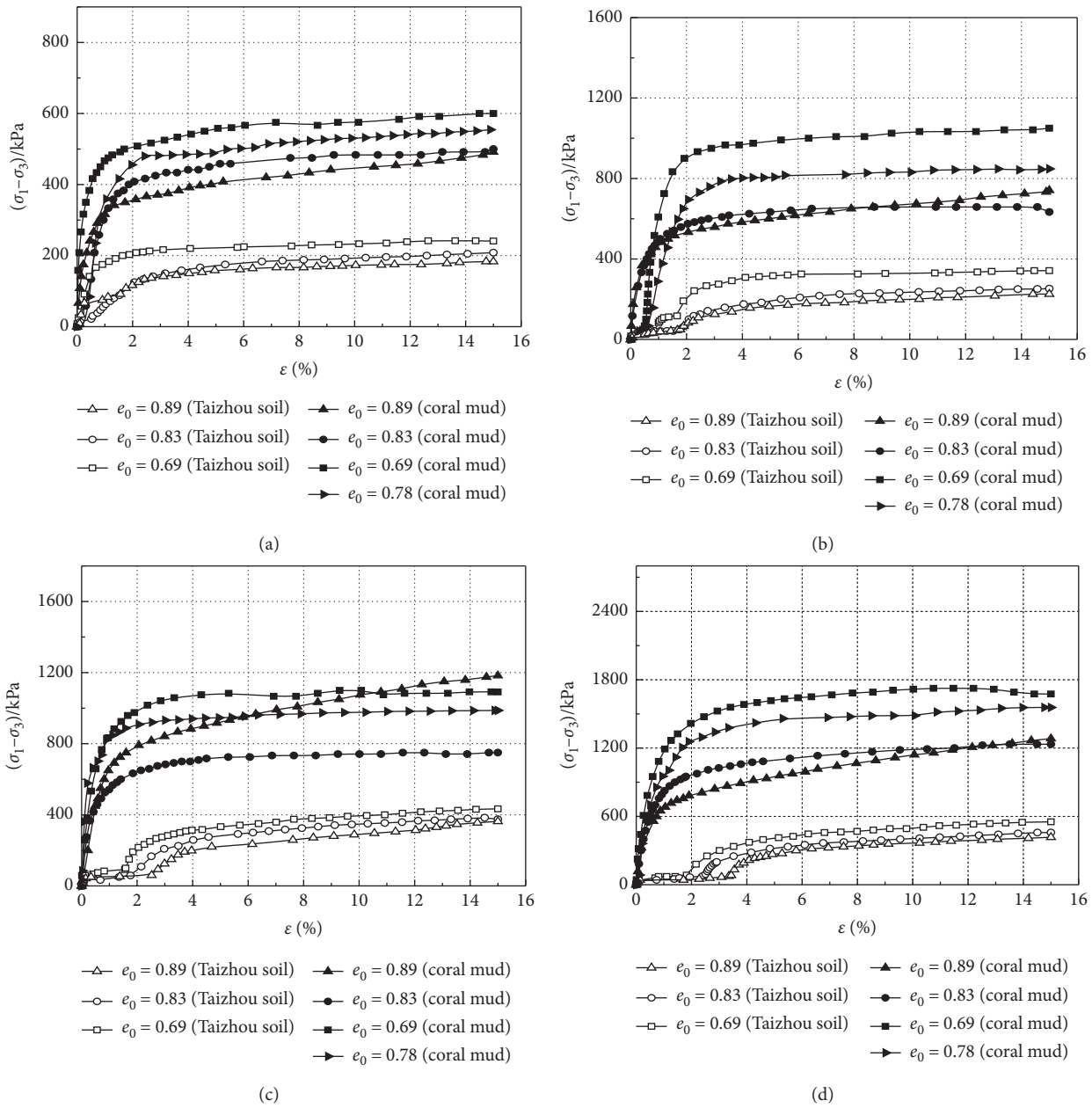

Figure 6: Stress-strain behaviour at different initial void ratios: (a) 100 kPa, (b) 200 kPa, (c) 300 kPa, and (d) 400 kPa.

Figure 7, coral mud has a better permeability with a higher dissipation rate of the pore pressure. Figure 8 presents the pore pressure at the shear stage. For Taizhou soil, the pores are similar to those of common clay that gradually develop to a peak after $\varepsilon = 2\%$ when the cement material is extruded and the particles are in direct contact. During the whole process, the pressures are above zero and are positively correlated with the confining pressure, and the difference value under adjacent confining pressure is up to 80 kPa. In contrast, the pore pressure of the coral mud first rises to a positive peak in a small range and then decreases to a stable negative value. The reason for the difference may be the mineral composition. Calcium carbonate is the main substance that makes up the coral mud, whose coefficient of permeability is higher than that of common clay. Therefore, the pore pressure of coral mud is hard to accumulate.

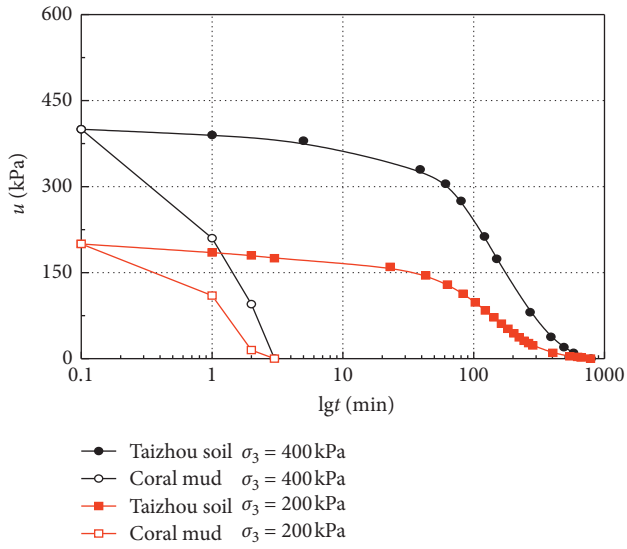

Figure 7: Pore pressure dissipation curve at the consolidation stage.

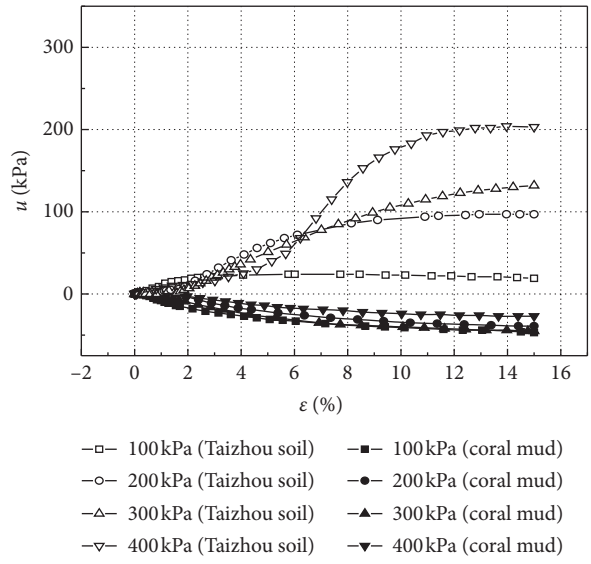

Figure 8: Pore pressures under different confining pressures.

3.2.2. Effects of the Initial Void Ratio. The pore pressures with different e_0 values are shown in Figure 9. The peak pore pressure of both samples increases with increasing e_0, but coral mud has a larger difference value with respect to the pore pressure as e_0 changes.

The pore pressure coefficient of sample failure is expressed as A_f to represent the final failure state. The relationships between A_f and e_0 are shown in Figure 10. It is clear that A_f and e_0 are linearly correlated, but the effect of e_0 varies under different p_0 values. When $p_0 = 100$ kPa, e_0 has the greatest effect, and A_f tends to be stable with increasing p_0, demonstrating that the two factors are not independent of each other in terms of their effects on A_f.

3.3. Effective Stress Path. In conventional triaxial tests, the effective stress path is usually expressed in the p'-q plane, where p' is mean effective stress and q is deviatoric stresses:

$$p' = \frac{\sigma_1 + 2\sigma_3}{3} - u = \frac{q}{3} + \sigma_1 - u,$$
$$q = \frac{1}{\sqrt{2}}\sqrt{(\sigma_1' - \sigma_2')^2 + (\sigma_2' - \sigma_3')^2 + (\sigma_3' - \sigma_1')^2}. \quad (1)$$

As shown in Figure 11, because of the unique pore pressure developments during undrained shearing, the effective stress path of coral mud is unlike the normally consolidated clay curve, which develops to the left [28] or the

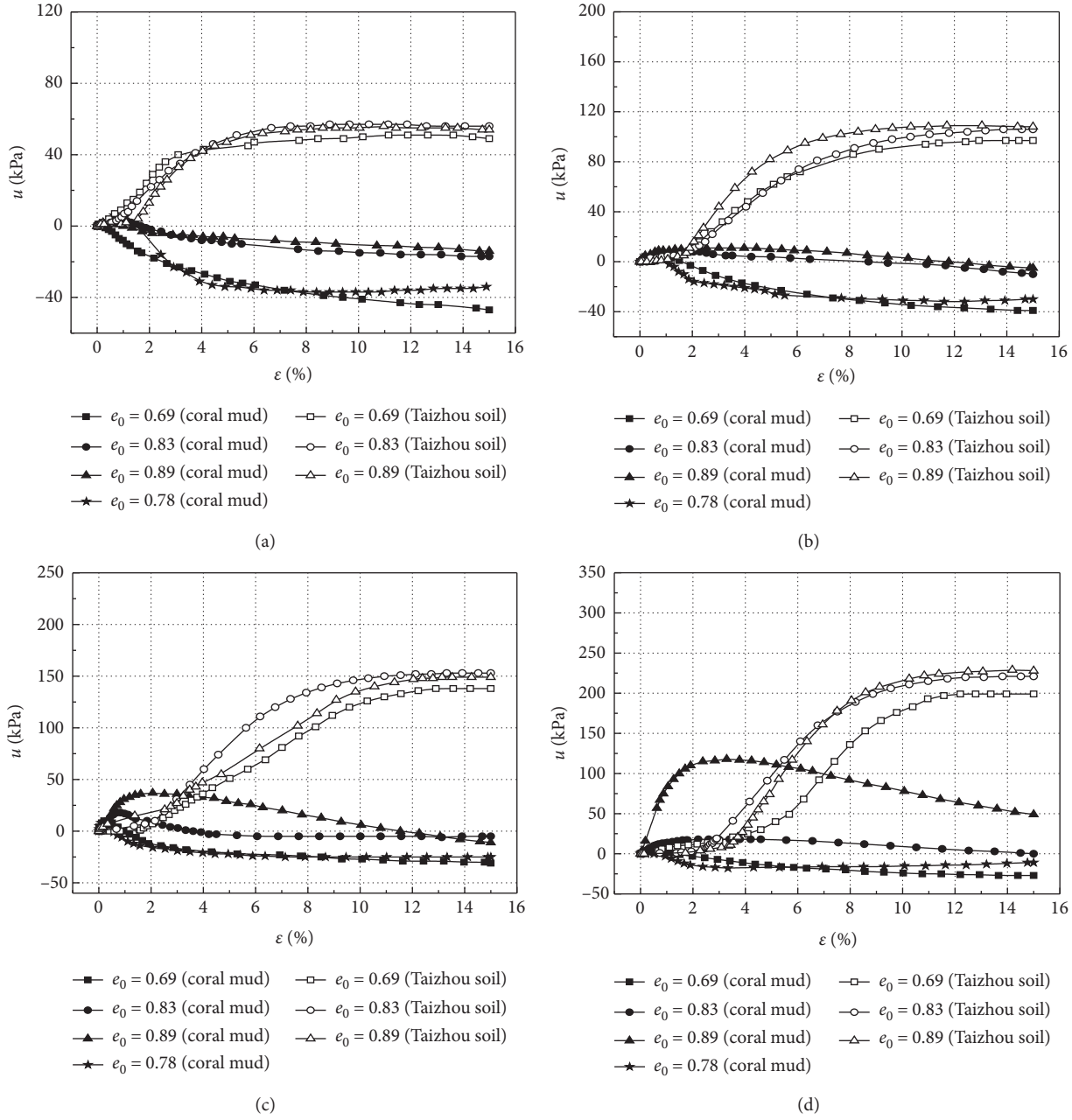

Figure 9: Pore pressures with different initial void ratios: (a) 100 kPa, (b) 200 kPa, (c) 300 kPa, and (d) 400 kPa.

general silt with an "*S*" curve [29]. Additionally, effective stress path is also not the same as the curve of over-consolidated clay, which obviously develops from right to left [30]. This path is similar to the total stress path curve and develops in a straight line. Although the stress path curves under different confining pressures are always similar, as confining pressure does not change the critical state of the soil mass, compared with Taizhou soil, the stress path of coral mud is less affected. The surge of pore pressure only exists at $e_0 = 0.89$ and $p_0 = 400$ kPa in the early shear phase, which causes a significant inflection point, and the inclination of other stress path curves of coral mud is almost equal.

Drawing the critical state line (CSL) according to the stress path, as shown in Figure 12, there is a good linear relationship between q_{cs} and p_{cs}', and it passes through the origin, which is consistent with the studies of other scholars. Figure 12 also shows the effective stress ratio M_{cs} at the critical state. It can be concluded that the M_{cs} value of Taizhou soil declines with increasing e_0, while that of coral mud first decreases and then slightly increases with increasing e_0, corresponding to the testing results that when

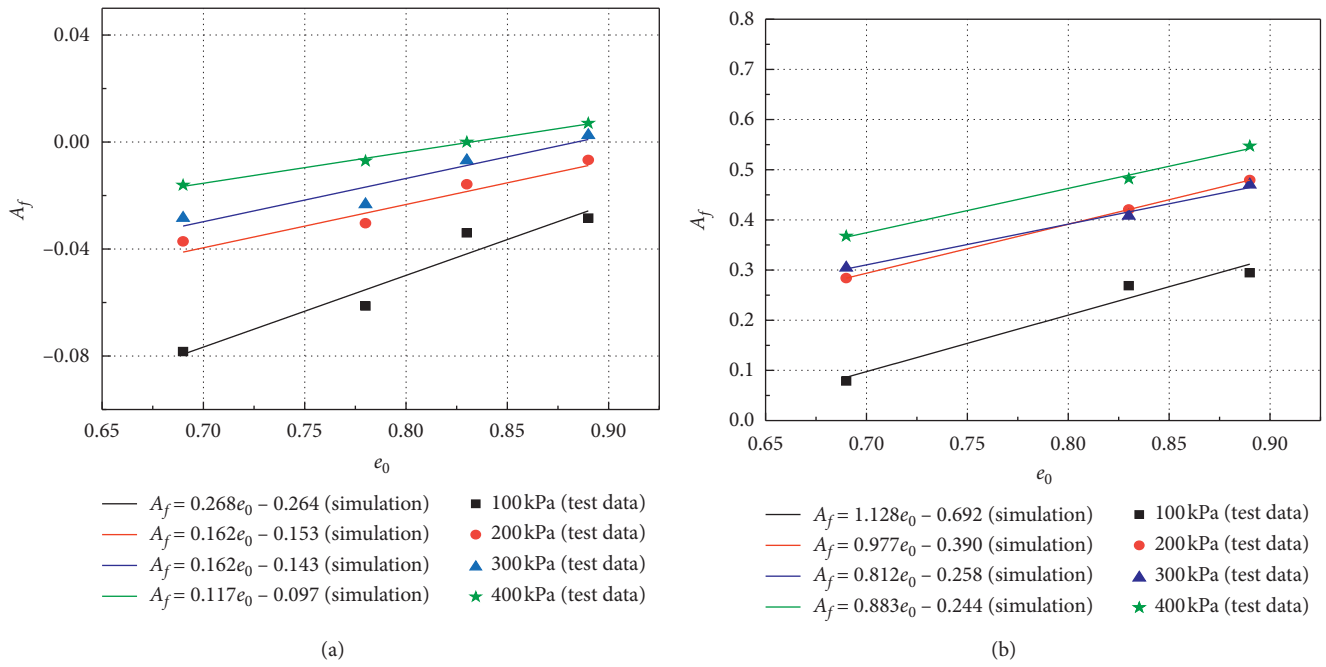

Figure 10: Relationship between a_f and e_0: (a) coral mud and (b) Taizhou soil.

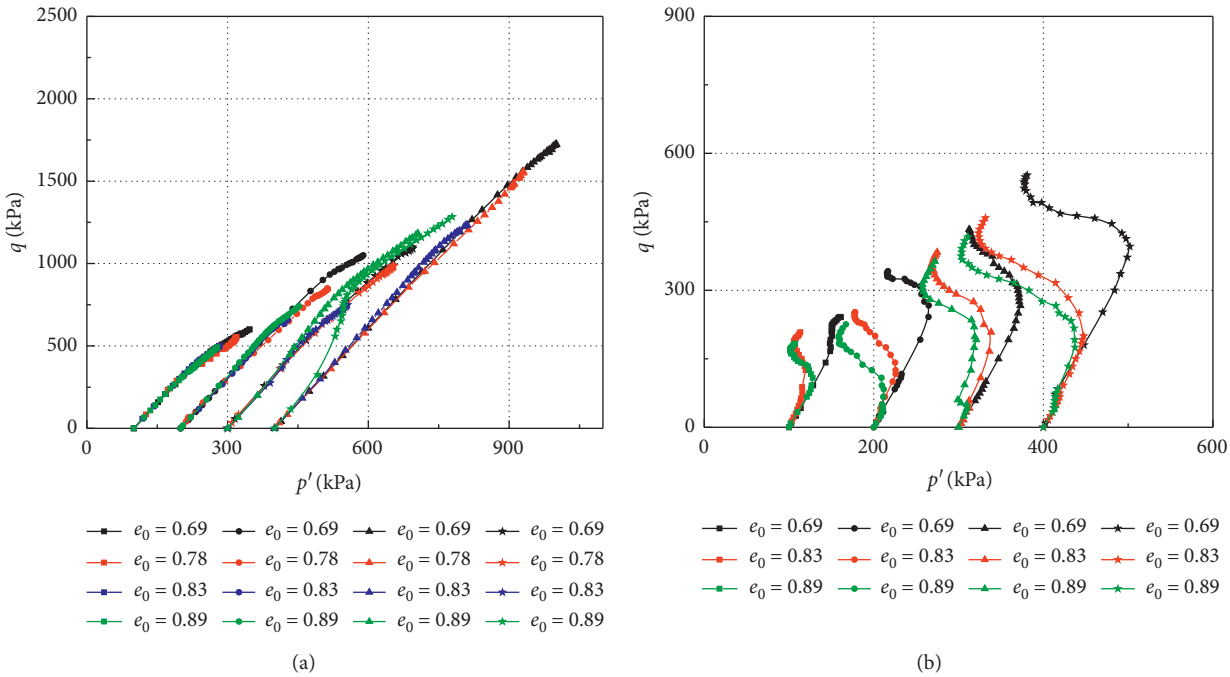

Figure 11: Effective stress paths with different initial void ratios: (a) coral mud and (b) Taizhou soil.

$e_0 = 0.89$, the deviatoric stress of coral mud continues to increase and finally is higher than the samples of $e_0 = 0.83$.

3.4. Friction Angle. The mobilized friction angle φ_m under the triaxial compression condition is defined as [31]

$$\sin \varphi_m = \frac{3\eta}{6 + \eta}, \tag{2}$$

where η is defined as the ratio of the deviatoric stress q to the effective mean stress p',

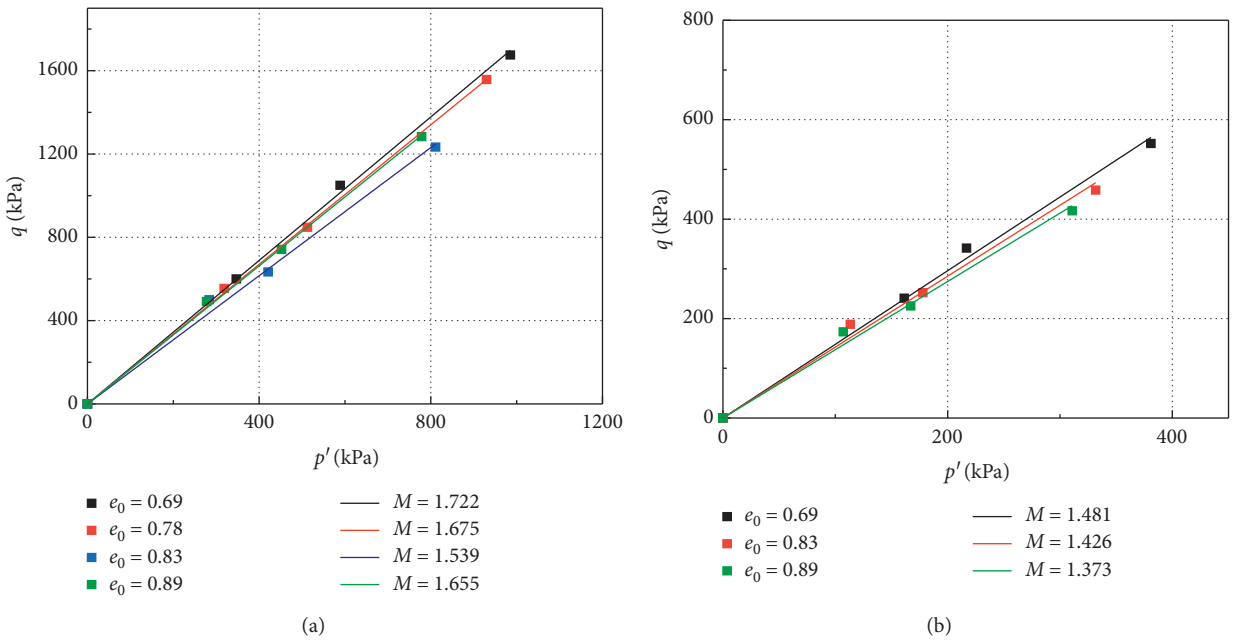

FIGURE 12: M_{cs} with different initial void ratios: (a) coral mud and (b) Taizhou soil.

$$\eta = \frac{q}{p'}. \tag{3}$$

The critical state friction angle φ_{cs} under the triaxial compression condition can be defined as

$$\sin \varphi_{cs} = \frac{3\eta_{cs}}{6 + \eta_{cs}}, \tag{4}$$

where η_{cs} is critical state stress ratio. The test data show that η only changes slightly when the strain is 15%. According to the critical state theory [32], the stress state under this strain could be considered a critical state.

The peak state friction angle φ_{ps} is defined as

$$\sin \varphi_{ps} = \frac{3\eta_{ps}}{6 + \eta_{ps}}, \tag{5}$$

where η_{ps} is the peak state stress ratio.

Figure 13 presents the mobilized friction angle of coral mud and Taizhou soil at different initial void ratios and pressures. The values of φ_{cs} and φ_{ps} are shown in Table 5. Similar to the stress-strain relationship, the mobilized friction angle-strain relationship of coral mud presents a platform shape, and when $e_0 = 0.89$, the curve has the property of overpenetration, while the other curves decrease with an increase in the initial void ratio. Most φ_{ps} values overlap with $\varphi_{cs,}$ and the remainder gradually approach the critical state. φ_{cs} of coral mud is much greater than that of Taizhou soil, and with increasing confining pressure, φ_{cs} of coral mud tends to disperse while the Taizhou soil tends to be dense, indicating that the initial void ratio has a minor effect on φ_{cs} of coral mud when the confining pressure is low.

As shown in Figure 14, φ_{cs} of Taizhou soil decreases first and then tends to be stable with an increase in the confining pressure, which indicates that an increase in the confining pressure gradually has less influence on the critical friction angle of Taizhou soil. Figure 15(b) also proves this conclusion, as the 300 kPa and 400 kPa curves almost coincide. In contrast, the confining pressure is an important parameter on φ_{cs} of coral mud. With an increase in the confining pressure, φ_{cs} first decreases and then increases when $e_0 = 0.78$ and $e_0 = 0.83$; first increases, then decreases, and then increases when $e_0 = 0.69$; and first decreases, then increases, and then decreases when $e_0 = 0.89$. Figure 15(a) illustrates that, at 100 kPa, the effect of the initial void ratio is minor as the curve approximates a straight line, which is consistent with the phenomenon of the high coincidence of φ_{cs} in Figure 13(a). Under the other confining pressures, φ_{cs} of coral mud first decreases and then increases with the increase in e_0.p_0 is the initial confining pressure, e_0 is the initial void ratio, $\varphi_{cs\text{-}c}$ is the critical state friction angle of coral mud, $\varphi_{ps\text{-}c}$ is the peak state friction angle of coral mud, $\varphi_{cs\text{-}T}$ is the critical state friction angle of Taizhou soil, and $\varphi_{ps\text{-}T}$ is the peak state friction angle of Taizhou soil.

3.5. Modulus. The initial elastic modulus E_{0i} is an important parameter, indicating the deformation behaviour of coral mud. It can be expressed as [33]

$$E_{0i} = \frac{q_\alpha}{\varepsilon_\alpha}, \tag{6}$$

where ε_a means the axial strain constrained within 0.1% for the initial slope of the stress-strain curve, where the deformation is supposed to be elastic.

E_{50} is the ratio of the stress of half of the peak stress of soil to the corresponding strain [34], which is defined as

$$E_{50} = \frac{0.5q_{ps}}{\varepsilon_{aps}}, \tag{7}$$

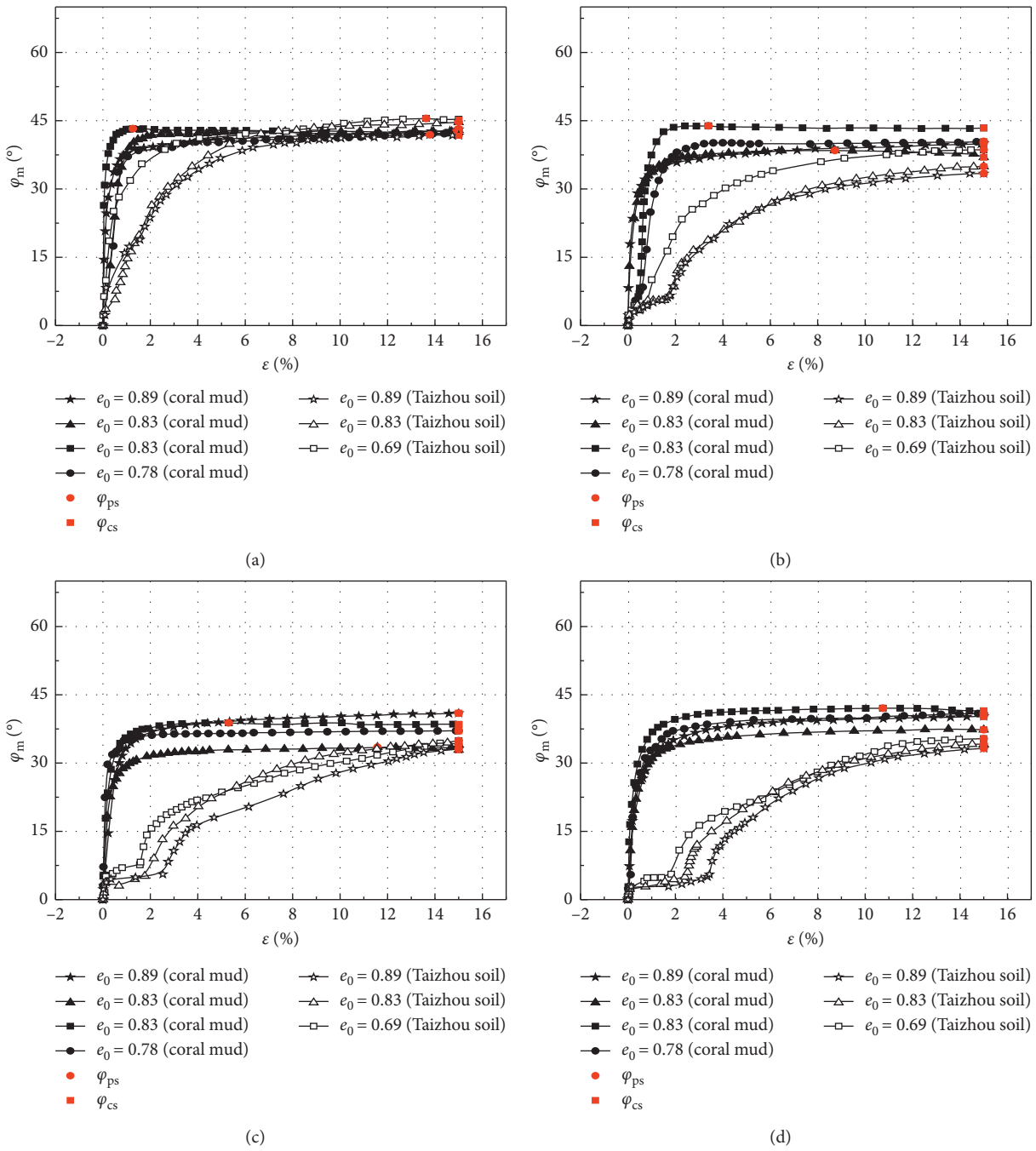

Figure 13: Mobilized friction angle of coral mud and Taizhou soil: (a) 100 kPa, (b) 200 kPa, (c) 300 kPa, and (d) 400 kPa.

where q_{ps} is peak stress during shearing and ε_{aps} is the corresponding strain. Table 6 presents the values of E_{0i} and E_{50}, and the relationships between E_{0i} and E_{50} and p_0 and e_0 are shown in Figures 16 and 17, respectively.

The initial elastic modulus of coral mud is nearly 10 times that of Taizhou soil, and the influences of p_0 and e_0 on coral mud are more obvious and regular. E_{0i} of coral mud can be expressed as a linear function of the logarithm of p_0 (R^2>0.98), while the slope of the fitted line equation does not change with the change in e_0; this result means that E_{0i} increases 139.55 MPa for every 100 kPa increase in lgp_0, independent of e_0. With an increase in e_0, E_{0i} of coral mud first decreases and then increases, but the growth range is small and the whole tends to be stable. The relationship between E_{0i} and e_0 under different confining pressures is similar, which also proves that the two factors are independent of each other.

Similar to the initial elastic modulus, the secant modulus of coral mud is also much higher than that of Taizhou soil. E_{50} increases linearly with increasing lgp_0, but the effects of p_0 and e_0 on E_{50} of coral mud are not completely independent. As shown in Figure 18, when e_0 = 0.89, the slope of

Table 5: Critical state friction angle and peak state friction angle of coral mud and Taizhou soil.

p_0 (kPa)	e_0	$\varphi_{cs\text{-}c}$ (°)	$\varphi_{ps\text{-}c}$ (°)	$\varphi_{cs\text{-}T}$ (°)	$\varphi_{ps\text{-}T}$ (°)
100	0.69	42.16	43.26	45.32	45.49
	0.78	42.94	42.94	—	—
	0.83	42.39	42.39	44.67	44.67
	0.89	43.09	43.09	41.75	41.90
200	0.69	43.41	43.87	38.60	38.60
	0.78	40.42	40.42	—	—
	0.83	36.96	38.47	34.94	34.94
	0.89	40.09	40.09	33.40	33.40
300	0.69	38.49	38.84	34.90	34.90
	0.78	37.08	37.08	—	—
	0.83	32.89	33.47	34.09	34.09
	0.89	40.95	40.95	33.10	33.10
400	0.69	41.48	42.06	35.35	35.35
	0.78	40.88	40.88	—	—
	0.83	37.34	37.34	34.16	34.16
	0.89	40.27	40.27	33.21	33.21

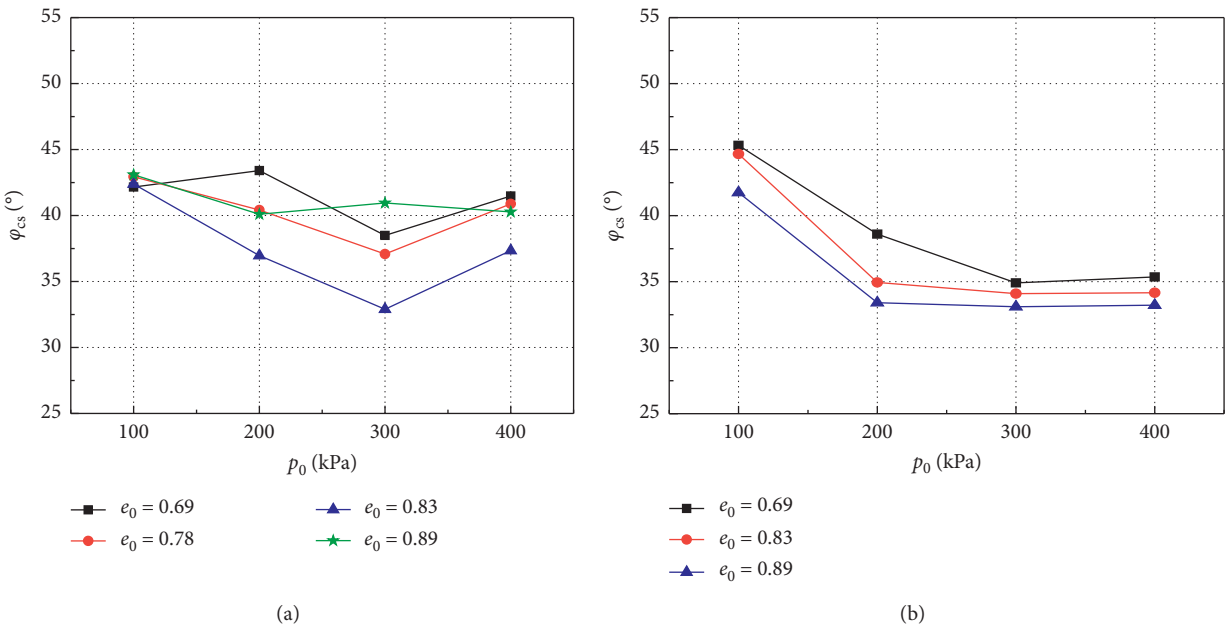

Figure 14: Relationship between φ_{cs} and p_0: (a) coral mud and (b) Taizhou soil.

the equation of the fitting line is much smaller than the others due to its special hardening law. Its stress increases continuously with the strain, the strain corresponding to 0.5 q_{ps} is larger, and the secant modulus decreases accordingly. This characteristic is also shown in Figure 19; with the increase in e_0 under different confining pressures, E_{50} curve tends to be concentrated from parallel.

3.6. Finite Element Simulation of the Stress-Strain Relationship. The Cam-Clay model is suitable for predicting the properties of normally consolidated and weakly overconsolidated clay under critical conditions [35], but whether it is suitable for coral mud remains to be studied. The model parameters λ, κ, and M obtained from one-dimensional compression tests and CU shear tests under confining pressures of 100 kPa–400 kPa were used to simulate the tests under 200 kPa, 400 kPa, and 600 kPa according to the Cam-Clay model.

3.6.1. Calculation of the Cam-Clay Model Parameters. Figure 20 shows the one-dimensional compression trial curve of coral mud. The curve is much gentler than the general compression curve, and the rebounding curve and unloading curve are close to coinciding, indicating that the compressibility and resilience of coral mud are very low.

The relationship among λ, κ, M, and e_0 was plotted according to the compression index (Table 7). As shown in

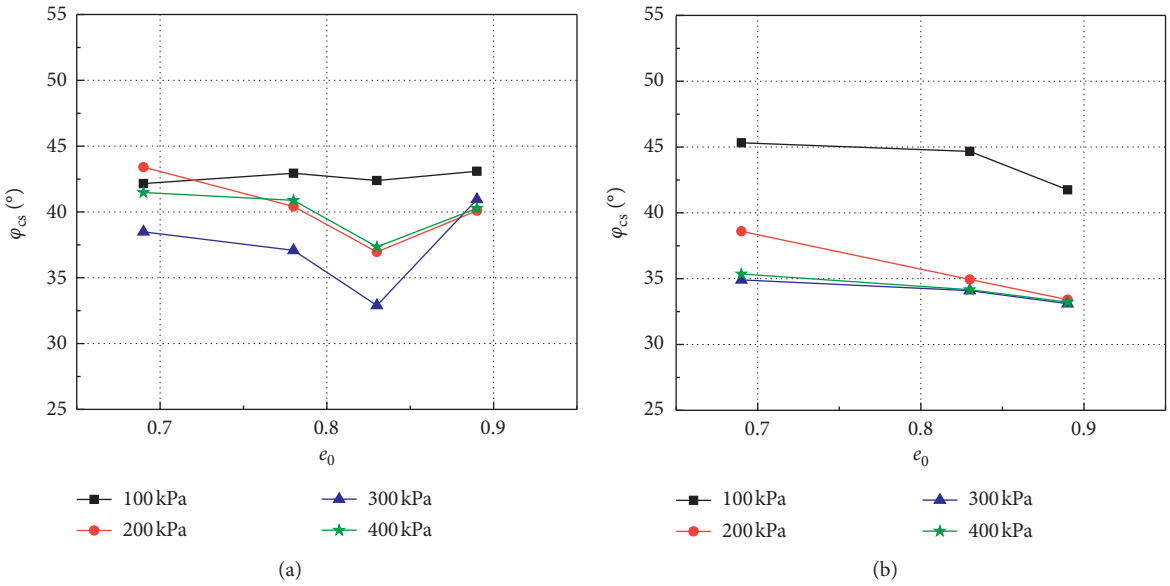

Figure 15: Relationship between φ_{cs} and e_0. (a) coral mud and (b) Taizhou soil.

Table 6: Initial elastic modulus and secant modulus at 50% of the peak strength of moral mud and Taizhou soil.

p_0 (kPa)	e_0	$E_{0i\text{-}c}$ (MPa)	$E_{50\text{-}c}$ (MPa)	$E_{0i\text{-}T}$ (MPa)	$E_{50\text{-}T}$ (MPa)
100	0.69	241.67	85.71	25.00	33.47
	0.78	158.33	56.74	—	—
	0.83	66.67	32.87	11.85	23.81
	0.89	103.71	52.25	16.67	20.83
200	0.69	350.33	135.66	33.33	9.83
	0.78	275.44	91.67	—	—
	0.83	166.67	86.02	26.67	5.26
	0.89	194.45	83.33	27.78	5.85
300	0.69	400.38	158.02	41.67	10.32
	0.78	338.05	121.03	—	—
	0.83	225.12	96.90	41.67	6.73
	0.89	250.13	74.89	37.88	6.11
400	0.69	441.67	185.61	41.67	12.21
	0.78	361.26	140.40	—	—
	0.83	355.71	113.03	44.45	7.21
	0.89	275.17	75.49	37.88	6.34

p_0 is the initial confining pressure, e_0 is the initial void ratio, $E_{0i\text{-}c}$ is the initial elastic modulus of coral mud, $E_{50\text{-}c}$ is the secant modulus of coral mud, $E_{0i\text{-}T}$ is the initial elastic modulus of Taizhou soil, and $E_{50\text{-}T}$ is the secant modulus of Taizhou soil.

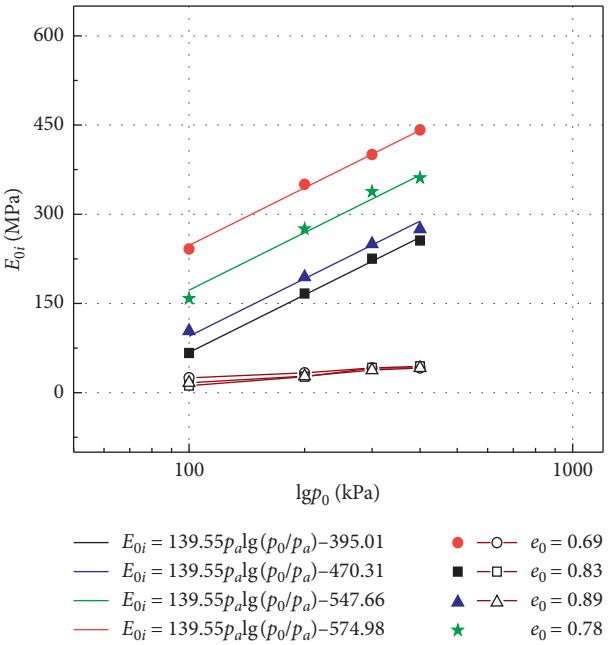

Figure 16: Relationship between E_{0i} and p_0.

Figure 21, λ is determined incrementally by a larger initial void ratio and κ fluctuates by approximately 0.0035, while M first decreases, then stabilizes, and slightly rises. These trends are different from those of Taizhou soil in which M linearly decreases with increasing e_0.

3.6.2. Simulation Results Analysis. According to the laboratory test results, the saturated coral mud sample with $e_0 = 0.89$ was subjected to a CU shear test simulation. The sample parameters were set as follows: diameter = 39.1 mm, height = 80 mm, confining pressures = 200 kPa, 400 kPa, and 600 kPa, $\nu = 0.38$, $\lambda = 0.065$, $\kappa = 0.003$, $M = 1.655$, $e_0 = 0.89$, and soil permeability coefficient = 1.13×10^{-6} cm/s.

Figure 22 presents the relationship between the test results and the simulation. Particularly, the predicted modulus in the early stage is smaller than the measured value, and the model

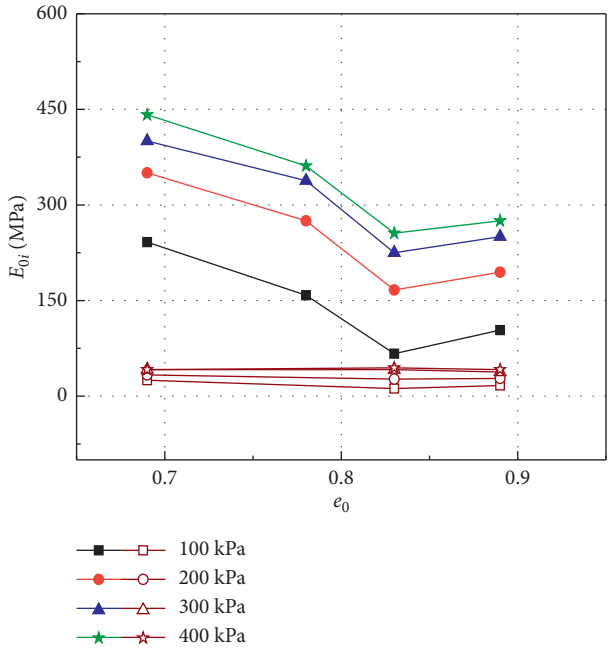

Figure 17: Relationship between E_{0i} and e_0.

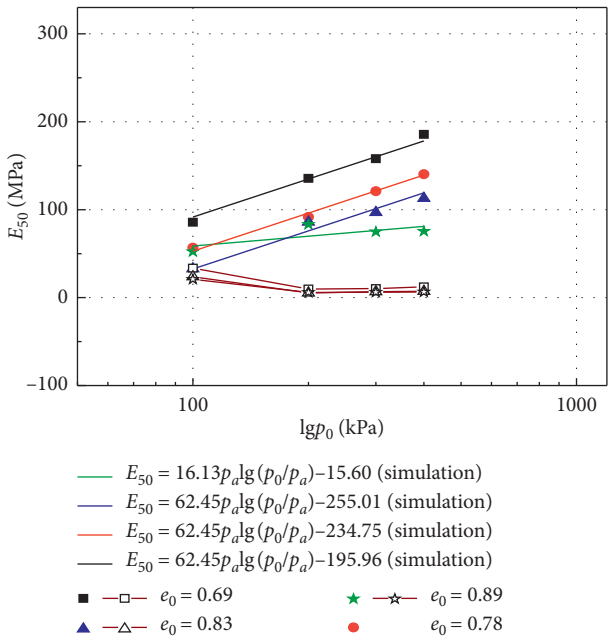

Figure 18: Relationship between E_{50} and lgp_0.

could not well reflect the hardening characteristics in the later stage. The unique microstructure of coral mud may be the reason why simulated results do not match the experimental data at low strain range. The irregular particles of coral mud come into direct contact from the beginning and stress increases rapidly at the initial stage of shear, different from common clay whose stress gradually increases at a slower rate. However, the error between the predicted peak and the

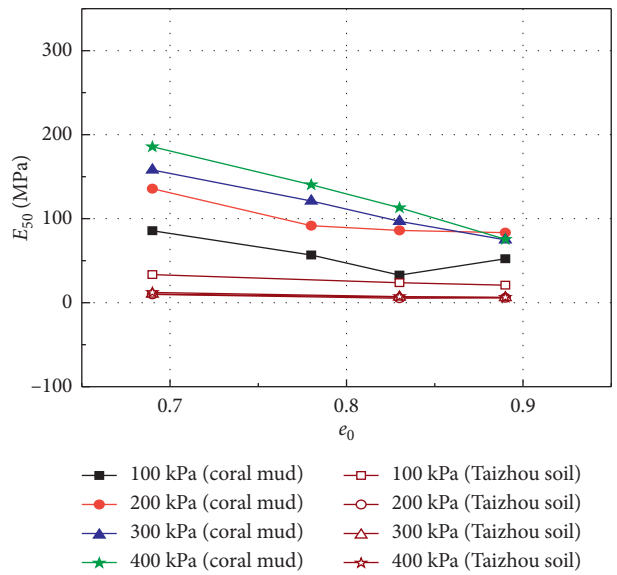

Figure 19: Relationship between E_{50} and e_0.

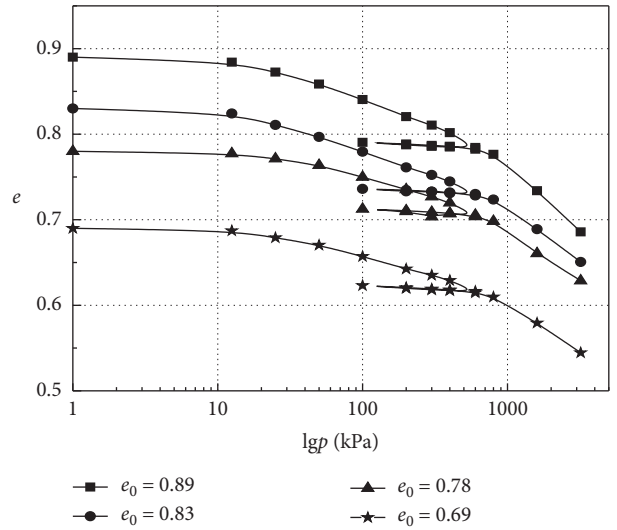

Figure 20: One-dimensional compression trial curve.

measured value is small, indicating that the Cam-Clay model has a certain reference for the stress-strain development of coral mud.

4. Conclusions

In this paper, SEM was implemented to better understand the microstructure of coral mud in the South China Sea. A series of triaxial tests were conducted to study the static shear strength behaviour. Cam-Clay was employed to simulate the stress-strain behaviour of the coral mud to verify the estimation ability. The main conclusions can be summarized as follows:

(1) The morphology of coral mud particles was extremely irregular, mainly strip and needle shaped. The strength of coral mud under the same confining

Table 7: Compression index of coral mud.

Initial void ratio e_0	Compression exponent cc	Swelling index C_s	λ	κ
0.69	0.1082	0.0086	0.0470	0.0037
0.78	0.1156	0.0090	0.0502	0.0039
0.83	0.1211	0.0078	0.0526	0.0034
0.89	0.1505	0.0077	0.0654	0.0033

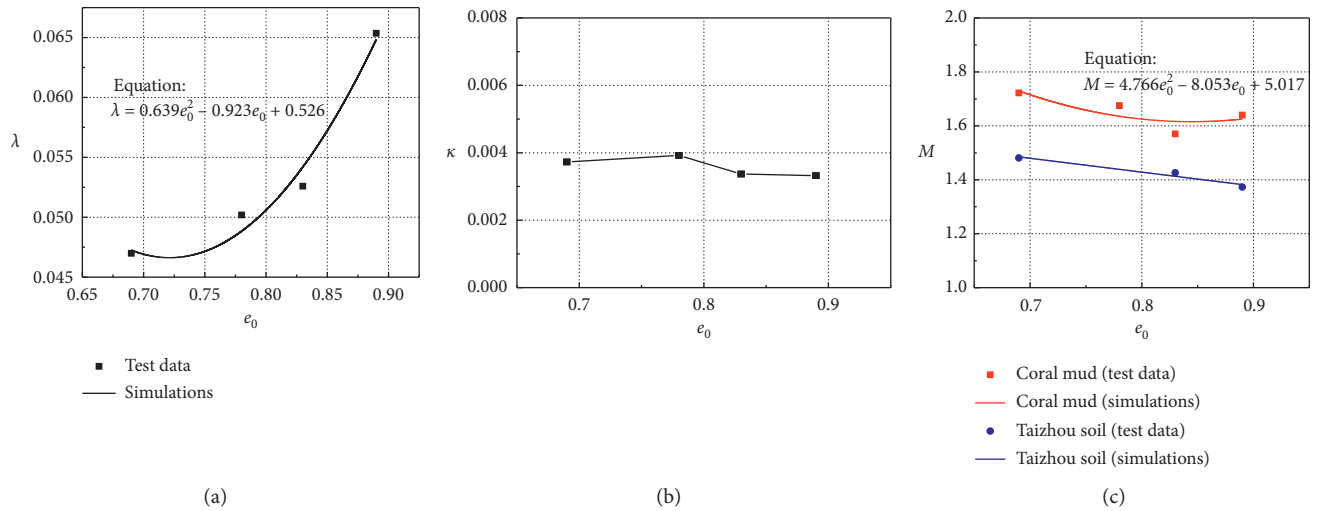

Figure 21: Relationship between the Cam-Clay model parameters and e_0. (a) Relationship between λ and e_0 of coral mud. (b) Relationship between κ and e_0 of coral mud. (c) Relationship between M and e_0.

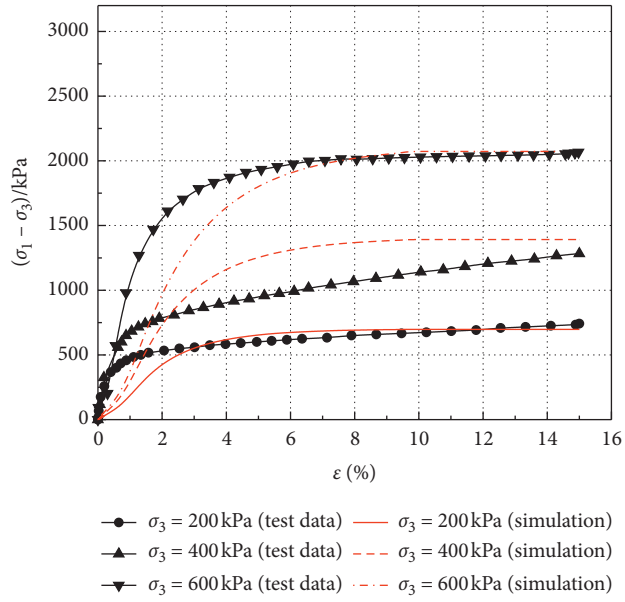

Figure 22: Relationship between the test results and simulation.

pressure was much higher than that of Taizhou soil. The initial void ratio e_0 and the initial confining pressure p_0 affected the strength and deformation characteristics. When $e_0 = 0.89$, the stress-strain plot exhibited an enhanced curve regardless of the confining pressure.

(2) The dissipation rate of the pore pressure in the consolidation and shear stages of coral mud was much higher than that of Taizhou soil, and the dilatancy characteristic was significant. When the

failure occurred, the pore pressure coefficient varied linearly with the initial void ratio.

(3) The effective stress path of coral mud was similar to the total stress path due to the unique pore pressure development.

(4) The peak friction angle of coral mud mostly coincided with the critical friction angle. The initial confining pressure had an important influence on the critical friction angle of coral mud. With the exception of 100 kPa, the critical friction angle of coral mud first declined and then developed with an increase in the initial void ratio.

(5) The initial elastic modulus of coral mud was nearly 10 times that of Taizhou soil. This result showed that there was a linear relationship between the initial elastic modulus E_{0i} and $\lg p_0$ as well as between the secant modulus E_{50} and p_0. The effects of p_0 and e_0 on the E_{0i} of coral mud were independent of each other.

(6) The value of parameter λ was determined incrementally by a larger initial void ratio, while the value of parameter M decreased smoothly first and then rose slightly; the selection of parameter κ was approximately 0.0035. The results suggest that the Cam-Clay model has a certain reference for predicting the stress-strain relationship of coral mud.

Notations

Cc: Coefficient of curvature
Cu: Coefficient of uniformity
R: Roundness
T: Aspect ratio
p_0: Initial confining pressure
ρd: Dry density
e_0: Initial void ratio
c: Coulomb-molar parameter
φ: Internal friction angle
A: Pore pressure coefficient
p': Mean effective stress
q: Deviatoric stress
p'_{cs}: Mean effective stress at the critical state
q_{cs}: Deviatoric stress at the critical state
M_{cs}: Effective stress ratio at critical state
φ_{cs}: Critical state peak state
φ_{ps}: Peak state peak state
ηps: Peak state stress ratio
E0$_i$: Initial elastic modulus
E50: Secant modulus at 50% of the peak strength
C_s: Swelling index
λ: Compression index
κ: Recompression index.

Data Availability

The data used to support the findings of this study are available from the corresponding author upon request.

Conflicts of Interest

The authors declare that they have no conflicts of interest.

Acknowledgments

The authors would like to acknowledge the financial support of the National Natural Science Foundation of China under Grant 51979087.

References

[1] H. Zhao, C. Song, Y. Zhu et al., *Environmental and Resource Characteristics and Development of Nansha Islands*, Earthquake Press, Beijing, China, 1993.

[2] X. Wang, "Study on the permeability characteristics of calcareous silty intercalation in the foundation of artificial island," *Rock and Soil Mechanics*, vol. 38, no. 11, pp. 3127–3135, 2017.

[3] Q. Jin, *Geology and Oil and Gas Resources in the South China Sea*, Geology Press, Beijing, China, 1989.

[4] Y. Wu, H. Yamamoto, J. Cui, and H. Cheng, "Influence of load mode on particle crushing characteristics of silica sand at high stresses," *International Journal of Geomechanics-ASCE*, vol. 20, no. 3, Article ID 04019194, 2020.

[5] J. Li, "Shear resistance of coral debris calcareous sand," *Geotechnical basis*, vol. 31, no. 2, pp. 226–230, 2017.

[6] Z. Sun and D. Huang, "Study on engineering properties of coral sand in Nansha Islands," *Journal of Engineering geology*, pp. 208–212, 2000.

[7] W. Qian, "Triaxial tests of calcareous sand on Mohr-coulomb strength characteristics," *Geotechnical foundation*, vol. 31, no. 2, pp. 321-322, 2017.

[8] R. WangC. Song et al., *Engineering Geology of Coral Reefs in Nansha Islands*, Science Press, Beijing, China, 1997.

[9] J. Zhang, "Experimental study on calcareous sand particle crushing under shear action," *Rock and Soil mechanics*, vol. 29, no. 10, pp. 2789–2793, 2008.

[10] J. Zhang, "Effects of particle crushing and dilatation on the shear strength of calcareous sand," *Rock and Soil mechanics*, vol. 30, no. 7, pp. 2043–2048, 2009.

[11] P. Zhang, B. Luo, and P. Liu, "Influence of moisture content on the strength characteristics of red clay," *Hydroelectricity*, vol. 45, no. 5, pp. 45–49, 2019.

[12] T. Zhang and D. Sun, "Relationship between shear strength and moisture content of guilin compacted red clay," *Journal of Shanghai University (Natural Science Edition)*, vol. 20, no. 05, pp. 586–595, 2014.

[13] J. Xu and S. Pan, "Experimental study on mechanical properties of soft soil changing with water content," *Journal of Huazhong University of Science and Technology*, vol. 19, no. 2, pp. 10–12, 2002.

[14] J. Li, "Stress-strain characteristics of clay with different moisture content under different test conditions," *Journal of Geotechnical Engineering*, vol. 28, no. 3, pp. 343–347, 2006.

[15] Y. Feng and Y. Zhang, "Experimental study on stress-water-strain relationship of remolded loess under directional shear stress path," *Journal of Qinghai University*, vol. 36, no. 1, pp. 47–53, 2018.

[16] C. Xiao, X. Li, and J. Zhang, "Effect of compaction degree and water content on performance of sandy silt," *Journal of Shenzhen University Science and Engineering*, vol. 34, no. 5, pp. 501–508, 2017.

[17] S. Wang, X. Lei, Q. Meng, J. Xu, M. Wang, and W. Guo, "Model tests of single pile vertical cyclic loading in calcareous sand," *Marine Georesources & Geotechnology*, pp. 1–12, 2020.
[18] Y. Shen, F. Zhaoyan, H. Liu, and An Li, "Experimental study on influence of initial concentration on settling velocity characteristics of turbidified liquid in coral mud deposition in the south China sea," *Journal of Geotechnical Engineering*, vol. 40, no. S2, pp. 22–26, 2018.
[19] Y. Shen, *Geotechnical Engineering Testing Technology*, Metallurgical Industry Press, Beijing, China, 2017.
[20] J. L. Wang, V. Vivatrat, and J. R. Rusher, "Geotechnical properties of Alaska oes silts," in *Proceedings of the 14th Annual Offshore Technology Conference, OTC 4412*, Houston, TX, USA, June 1982.
[21] S. Iravani, *Geotechnical Characteristics of Penticton Silt*, University of Alberta, Edmonton, Canada, 1999.
[22] T. L. Brandon, A. T. Rose, and J. M. Duncan, "Drained and undrained strength interpretation for low-plasticity silts," *Journal of Geotechnical and Geoenvironmental Engineering*, vol. 132, no. 2, pp. 250–257, 2006.
[23] Z. Zhu and S. Liu, "Triaxial test of silt and its stable soil," *Rock and Soil Mechanics*, vol. 26, no. 12, pp. 1967–1971, 2005.
[24] X. Tu and S. Wang, "Description of particle shape parameters in image analysis," *Journal of Geotechnical Engineering*, vol. 26, no. 5, pp. 659–662, 2004.
[25] C. F. Mora and A. K. H. Kwan, "Sphericity, shape factor, and convexity measurement of coarse aggregate for concrete using digital image processing," *Cement and Concrete Research*, vol. 30, no. 3, pp. 351–358, 2000.
[26] M. L. Hentschel and N. W. Page, "Selection of descriptors for particle shape characterization," *Particle & Particle Systems Characterization*, vol. 20, no. 1, pp. 25–38, 2003.
[27] l. Jiang, *Study on Mechanical Properties of Calcareous Sand in South China Sea*, Chengdu University of technology, Chengdu, China, 2014.
[28] M. Jiang, "A new perspective of modern soil mechanics research -- macro and micro soil mechanics," *Journal of Geotechnical Engineering*, vol. 41, no. 2, pp. 195–254, 2019.
[29] G. Li, *Higher Soil Mechanics*, tsinghua university press, Beijing, China, 2nd edition, 2016.
[30] M. Braja, *Das. Advanced Soil Mechanics*, The University of Texas, El Paso, TX, USA, 1983.
[31] J. Qian and Z. Yin, *Geotechnical Principle and Calculation*, China water resources and hydropower press, Beijing, China, 2nd edition, 2000.
[32] K. Wang, *Triaxial Experimental Study on Consolidation and Unloading Strength Characteristics of Silt in Hangzhou*, Zhejiang University of Science and Technology, Zhejiang, China, 2019.
[33] H. Bingbing, *Experimental Study on Small Strain Shear Modulus and Shear Characteristics of Anisotropic Superconsolidated Wenzhou Soft Clay*, Harbin Institute of Technology, Harbin, China, 2018.
[34] Y. Xiao and S. M. ASCE, "Strength and deformation of rockfill material based on large-scale triaxial compression tests. I: influences of density and pressure," *Journal of Geotechnical and Geoenvironmental Engineering*, vol. 140, no. 12, Article ID 04014070, 2014.
[35] K. H. Roscoe, A. N. Schofield, and A. Thurairajah, "Yielding of clays in states wetter than critical," *Géotechnique*, vol. 13, no. 3, pp. 211–240, 1963.